BIOCHEMISTRY

 Volume 45, Number 43 October 31, 2006

Articles

The Crystal Structure of the BAR Domain from Human Bin1/Amphiphysin II and Its Implications for Molecular Recognition†

Eva Casal,‡ Luca Federici,§ Wei Zhang,‡ Juan Fernandez-Recio,|| Eva-Maria Priego,‡ Ricardo Nuñez Miguel,‡ James B. DuHadaway,⊥ George C. Prendergast,⊥ Ben F. Luisi,*,‡ and Ernest D. Laue‡

Department of Biochemistry, University of Cambridge, 80 Tennis Court Road, Cambridge CB2 1GA, U.K., Ce.S.I. Centro Studi sull'Invecchiamento and Dipartimento di Scienze Biomediche, Università di Chieti "G. D'Annunzio", Via dei Vestini 31, 66013 Chieti, Italy, Institute of Biomedical Research, Barcelona Science Park, Josep Samitier 1-5, 08028 Barcelona, Spain, and Lankenau Institute for Medical Research, 100 Lancaster Avenue, Wynnewood, Pennsylvania 19096

Received April 13, 2006; Revised Manuscript Received July 21, 2006

ABSTRACT: BAR domains are found in proteins that bind and remodel membranes and participate in cytoskeletal and nuclear processes. Here, we report the crystal structure of the BAR domain from the human Bin1 protein at 2.0 Å resolution. Both the quaternary and tertiary architectures of the homodimeric Bin1BAR domain are built upon "knobs-into-holes" packing of side chains, like those found in conventional left-handed coiled-coils, and this packing governs the curvature of a putative membrane-engaging concave face. Our calculations indicate that the Bin1BAR domain contains two potential sites for protein−protein interactions on the convex face of the dimer. Comparative analysis of structural features reveals that at least three architectural subtypes of the BAR domain are encoded in the human genome, represented by the Arfaptin, Bin1/Amphiphysin, and IRSp53 BAR domains. We discuss how these principal groups may differ in their potential to form regulatory heterotypic interactions.

The BAR domain was first identified by its common occurrence in vertebrate Bin1 and Amphiphysins and in the *Saccharomyces cerevisae* Rvs proteins (*1*). The family has now expanded to include many other BAR-containing proteins, such as endophilins, sorting nexins, nadrins, centaurins, and oligophrenins, which are mostly involved in membrane binding or remodeling events (*2*). The structures of the BAR domains of *Drosophila* Amphiphysin, human Arfaptin2, and murine Endophilin have been published recently, in addition to the more distantly related IRSp53/MIM domain (IMD[1]) of human IRSp53 (*2*−*5*).

Architecturally, the BAR domain is a kinked, trihelical coiled-coil that forms a banana-shaped homodimer with a positively charged concave face. This face is proposed to engage curved membranes through electrostatic attraction, and so may induce curvature in otherwise planar membranes.

† This work was supported by the Wellcome Trust. E.C. was a recipient of a Gates-Cambridge Trust scholarship, L.F. was a recipient of a Marie Curie fellowship, and E.-M.P was supported by a grant from Ministero Español de Educacion y Ciencia. J.F.-R. was supported by a Curie European Reintegration Grant and by the Ramon y Cajal Program of the Spanish Ministry of Science and Technology. G.C.P. is supported by grants from the NIH, DoD Breast and Prostate Cancer Research Programs, and the Lankenau Hospital Foundation.

* Corresponding author. E-mail: bfl20@mole.bio.cam.ac.uk. Phone: 44-1223-766019. Fax: 44-1223-766002.

‡ University of Cambridge.

§ Università di Chieti "G. D'Annunzio".

|| Institute of Biomedical Research, Barcelona Science Park.

⊥ Lankenau Institute for Medical Research.

[1] Abbreviations: IMD, IRSp53/MIM domains; ODA, optimal docking area.

10.1021/bi060717k CCC: $33.50
Published on Web 10/10/2006

In vitro, the BAR domain causes liposomes to elongate dramatically, a process which has been described as "tubulation". Mutation of the positively charged residues in the concave face inhibits this tubulation activity (*2*). *In vivo*, overexpression of the BAR domain of human Amphiphysin II in tissue culture cells causes invagination of the plasma membrane to form internal tubules that resemble the T-tubules of skeletal muscle involved in excitation-contraction coupling (*6*). As well as the BAR domain, the N-terminal region also plays an important role in membrane bending (*7*). This auxiliary region is likely to undergo a random coil to helical transition on engagement with the membrane (*2*).

Amphiphysins are BAR-containing proteins proposed to function chiefly in endocytosis and other membrane remodeling processes (*7*, *8*). They are composed of an N-terminal BAR domain with an additional N-terminal helix, followed by a variable central region which shows significant variation in different alternatively spliced protein isoforms, and a C-terminal SH3 domain. Mammalian Amphiphysin I proteins are expressed in the brain and nervous system, and they contain domains that bind components of the endocytic machinery, such as clathrin, adaptor protein complex 2 (AP2) *via* the central CLAP domain, and dynamin and synaptojanin *via* the C-terminal SH3 domain (*9*). Mammalian Bin1/Amphiphysin II proteins include nearly a dozen splice isoforms that have more complex patterns of expression than Amphiphysin I. The Amphiphysin II isoforms expressed in the brain and nervous system most closely resemble Amphiphysin I in structure, localization, and function in endocytosis. In contrast, the Bin1 isoforms expressed in other cells throughout the body lack brain-specific segments, do not function in endocytosis, and display distinct patterns of cellular localization (*1*, *10*−*14*). Recent evidence suggests that Bin1/Amphiphysin II may function in intracellular vesicle trafficking (*10*, *15*). One tissue-specific isoform of Bin1 is expressed at very high levels in skeletal muscle where it contributes to formation of the specialized membranes of the T-tubule system (*6*, *14*). Notably, the *Drosophila* Amphiphysin gene (which resembles mammalian Bin1/Amphiphysin II most closely) is dispensable for endocytosis but essential for proper organization of the T-tubule system in muscle (*16*−*18*). In the mouse, a homozygous knockout of the Bin1/Amphiphysin II gene, leads to severe cardiac muscle disorganization (*19*), in support of a role in maintaining the T-tubule system. In this regard, it is interesting to note that the upstream element of the human Amphiphysin II gene contains a consensus binding site for MyoD, the master regulator of muscle cell differentiation (*13*). Collectively, these observations implicate the BAR domain in recognizing and remodeling membranes, and suggest a key role of Bin1-type proteins in maintaining muscle T-tubule membrane structure.

In addition to the potential for membrane binding, many BAR domain proteins have been shown to interact, either directly or indirectly, with small G-proteins (*20*). For instance, Arfaptin binds to Rac, Arf1, Arf3, and Arf6 (*3*). The proteins known as the APPL group, which also contain an N-terminal BAR domain, interact with the small G-protein Rab5 (*21*). The more distantly related IRSp53, a protein involved in lamellopodium formation, interacts with Rac (*22*). These observations suggest that BAR domains may serve as a general platform for binding small G-proteins (*20*). The structure of the Arfaptin−Rac complex (*3*) shows that the small G-protein binding site and the putative membrane-binding face of the BAR domain occur in the same region of the protein. Thus, the membrane-binding activity of the BAR domain could be modulated by regulatory interactions with small G-protein or other partner proteins (*20*).

Here we describe the 2.0 Å resolution structure of the BAR domain of the human Bin1 protein (Bin1BAR), an isoform of Amphiphysin II. We have compared the Bin1BAR structure to other BAR domain structures and analyzed their curvature and potential for binding small G-proteins. The implications of these observations for the function of BAR domains in different proteins are discussed.

EXPERIMENTAL PROCEDURES

Expression and Purification of Bin1BAR. The BAR domain of human Bin1/Amphiphysin II (Bin1BAR, residues 1−251) was cloned into the bacterial expression pET14b vector. The histidine tagged recombinant protein was expressed in *Escherichia coli* BL21(DE3) and purified in the soluble form. Cell cultures were grown at 37 °C to OD 600 of 1.0 and induced with 1 mM IPTG for 4 h. The cells were harvested by centrifugation and resuspended in Tris lysis buffer (40 mM Tris-Cl pH 8.0, 100 mM NaCl, 10 mM imidazole) containing protease inhibitors. The cells were then lysed on ice using a Misonix ultrasonicator, and the cell lysate was clarified by centrifugation. The supernatant was subsequently loaded onto an immobilized nickel column equilibrated in lysis buffer, and His-Bin1BAR was eluted with a gradient of elution buffer (40 mM Tris-Cl pH 8.0, 100 mM NaCl, 10−400 mM imidazole).

The His tag was then removed with thrombin (0.5 unit/mg of protein, 4 h, room temperature (RT)), and the untagged Bin1BAR was further purified by gel filtration, using a Superdex-75 column equilibrated with gel filtration buffer (25 mM Tris-Cl pH 7.5, 150 mM NaCl). Approximately 50 mg of pure, soluble protein was obtained from 1 L of culture.

Analysis of Bin1BAR and Small G Protein Interaction by Size-Exclusion Chromatography and Pull-Down Analyses. The Bin1BAR was expressed and purified as described above. Small G-protein Rac was expressed and purified from *E. coli* BL21(DE3) as described earlier (*23*). Three purified small G-proteins, Rab6B, Rab9B, and Rab17, were kind gifts from Dr. M. Dyson at the Sanger Centre, Cambridge. Either 25 μL of single protein or 50 μL of preincubated mixture of Bin1BAR:small G-protein at a 2:1 molar ratio was applied onto a Superdex 200 P.C. 3.2/30 analytical column pre-equilibrated with gel filtration buffer at 4 °C on an Ettan LC system (GE healthcare). The traces of each single Bin1BAR and small G-protein and their mixture were superposed to verify any change in the peak position which will reflect the complex formation. Peaks were analyzed by SDS−PAGE. In pull-down experiments, His-tagged Bin1BAR was absorbed onto Ni-NTA superflow beads (Novagen) which were pre-equilibrated with Bin1Bar protein buffer. Bin1BAR bound to the beads was washed 4 times with purification buffer. For the interaction, 50 μL of Bin1BAR bound to the beads was added to 400 μL of each small G-protein at 100 μg/mL and incubated at 4 °C for 2 h with gentle rotation. The beads were spun down and washed 4 times with buffer. Bin1BAR and any interacting proteins were analyzed on 12% Bis-Tris NuPAGE denaturing gels.

Crystallization. Human Bin1BAR was crystallized by the hanging drop vapor diffusion method. The protein was concentrated to approximately 25 mg/mL in gel filtration buffer and mixed with an equal volume of the reservoir solution containing 20% monomethylether-PEG550, 100 mM Tris-Cl pH 8.0, 100 mM NaCl. Crystals appeared after approximately 2 weeks at 20 °C and reached final dimensions of 0.7 × 0.2 × 0.2 mm^3. Crystals were immersed in crystallization buffer containing 20% v/v glycerol as a cryoprotectant, before freezing in a nitrogen stream at 100 K for data collection. Crystals derivatized with xenon were placed in a pressure cell under 15 bar for approximately 20 s before flash-freezing.

Structure Determination. Bin1BAR crystals displayed anisotropic diffraction and usually diffracted to a maximum of 3.0 Å resolution. However, a good quality crystal was found that had been derivatized with xenon, and data were collected to 2.0 Å resolution from this specimen at the ESRF in Grenoble, France, on beamline ID14-4. The improvement of data quality may be due to dehydratation of the crystal due to exposure to a high pressure of xenon prior to freezing. Data were also collected from a selenomethionine derivative. The fluorescence spectra indicated a mixed oxidation state for the Se, and the derivative was not satisfactory for experimental phase determination; however, the positions of the Se atoms were useful for corroborating the modeling using anomalous Fourier syntheses. The data were processed with Denzo and Scalepack (*24*). Crystals belong the space group $P2_1$ with cell dimensions $a = 69.92$ Å, $b = 59.09$ Å, $c = 75.01$ Å, and $\beta = 117.53°$. Two molecules were predicted to occupy the asymmetric unit of the crystal according to Matthews calculations, with a solvent content of ~50%. The structure was solved by molecular replacement using the xenon derivative data set as a native data set. The structure of the Amphiphysin BAR domain protomer from *Drosophila melanogaster* (PDB entry 1URU) was used as a search model (*2*). The dyad axis protocol as implemented in the program MolRep (*25*) was used to obtain the correct solution. Refinement was initially performed with CNS (*26*) while REFMAC5 (*27*) was used in the later stages. Iterative cycles of model building with QUANTA (Molecular Structure Inc.) or Coot (*28*) and restrained refinement were performed. The final model contains two monomers in the asymmetric unit (chain A, residues 52−249; chain B, residues 50−250); the physiological dimers are generated through crystallographic symmetry. Due to poor definition of the electron density, residues were not modeled for the first 51 residues of chain A and 49 residues of chain B, residues 173−179 in the loop between helices 2 and 3 of chain A, the two C-terminal residues of chain A, and the C-terminal residue of chain B. Density was found for two partially occupied xenon atoms lying at the interface between two symmetry related molecules in the physiological dimer. Statistics from data processing and model refinement are shown in Table 1. Coordinates and structure factors have been deposited within the Protein Data Bank (http://www.rcsb.org) with accession code 2FIC.

Computational Analyses. The optimal docking area (ODA) computations used the procedure of Fernandez-Recio et al. (*29*). The knobs-into-holes interactions of the helices were analyzed with the program SOCKET (http://www.biols.susx.ac.uk/Biochem/Woolfson/html/coiledcoils/socket/) (*30*) using an 8 Å cutoff. Structure superpositions were performed using programs COOT (*28*) or ALIGN (*31*). Figure 3 was prepared using program GRASP (*32*). Figures were otherwise prepared using program PyMOL (*33*).

Table 1: Summary of Crystallographic Data and Refinement

radiation source	ESRF ID14.4
wavelength (Å)	0.9393
resolution (Å)	30.00−2.00
(last shell)	2.07−2.00
R_{merge}	0.079 (0.257)
unique reflections	36 811
completeness	98.3 (84.8)
multiplicity	4.2
$I/\sigma(I)$	37.2
cell dimensions	$a = 69.922$ Å $b = 59.086$ Å $c = 59.086$ Å $\beta = 117.534°$
space group	$P2_1$
Refinement	
R (working set)	0.2303
R_{free} (test set)	0.2798
rms deviations	
bond lengths (Å)	0.018
bond angles (deg)	1.642
Ramachandran statistics	
% of residues in allowed regions	99.7
% of residues in generously allowed regions	0.3
% of residues in not allowed regions	0
Model	
amino acids	chain $A = 52-249$; chain $B = 50-250$
water molecules	200
xenon atoms	2

Modeling. The sequence of human Amphiphysin II including the inserted region was analyzed by the program FUGUE (*34*), which searches for likely homologues based on a sequence−structure comparison. This query yielded a single structure (human squalene synthase, 1EZF) with a stretch of sequence that aligned to the inserted region in Amphiphysin II described above (*35*) (Figure 7). This stretch of sequence (amino acids 232−278) constituted an α-helical region that connected two α-helices of the protein together, as is predicted to be the case for the inserted region of Amphiphysin II. In addition, the secondary structure prediction for the insert and the structure of this region of human squalene synthase matched reasonably well. The structure of this connecting segment was then manually superposed to the Bin1BAR structure, and this was used as the template from which the model of Bin1BAR plus the insertion was made.

The model was prepared in MODELLER (*36*). Missing side chains of incomplete pdb models were rebuilt using the program SCWRL (*37*). Validation of the structure was carried out as for the Bin1BAR structure using PROCHECK (*38*), Verify 3D (*39*), and Molprobity (*40*). All amino acids fell within allowed regions of the Ramachandran plot.

RESULTS

Overall Structure. The structure of Bin1BAR was determined by molecular replacement using the structure of the *Drosophila* Amphiphysin BAR protomer (*2*) as a search

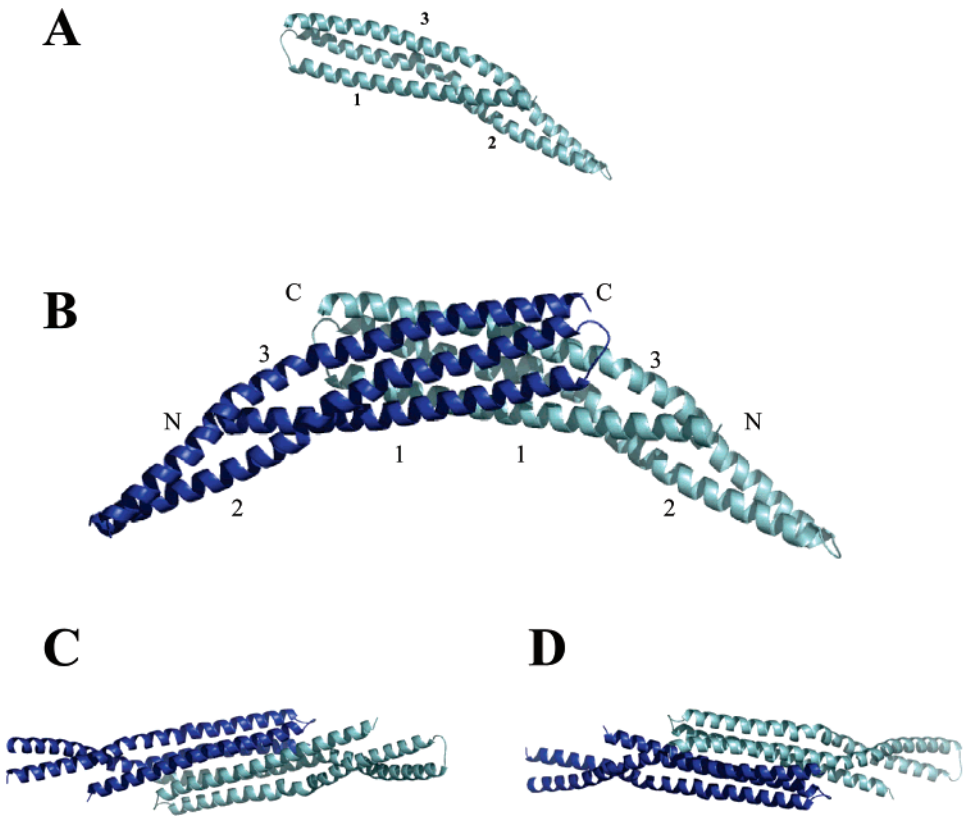

FIGURE 1: Overall structure of the BAR domain of Bin1. (A) Protomer of Bin1BAR. The numbering refers to the helices, starting from the N terminus. (B) The Bin1 homodimer, generated from crystallographic symmetry. The protein forms a banana-shaped homodimer. (C) View of the concave face of the dimer. (D) View of the convex face of the dimer.

model. Two molecules are present in the asymmetric unit of the Bin1BAR crystal, and the physiological dimer is obtained by applying crystallographic symmetry.

Bin1BAR forms a completely α-helical, symmetric homodimer with an elongated, curved shape (Figure 1). Both the tertiary and the quaternary structures of Bin1BAR are congruent with the structure of other BAR domains known to date (Figure 2), in particular with the structure of *Drosophila* Amphiphysin BAR domain (Figure 2B) and the murine Endophilin BAR domain (Figure 2C) (*2*, *5*). The structural similarity is striking given the comparatively small sequence identities of the proteins (Table 2 and figure in Supporting Information). The key characteristic of the BAR domain fold is "knobs-into-holes" interactions of nonpolar side chains, similar to those proposed by Crick for conventional left-handed coiled-coils. These coiled-coil interactions occur not only within the protomers but also at the dimer interface between protomers. The helical associations define the radius of curvature of the putative membrane engaging face.

The architecture of the Bin1BAR dimer can be deconvoluted into three main segments that differ in the number of bundled helices (Figure 2A). The simplest is composed of two α-helices at the extreme ends of the dimer (yellow helices in Figure 2A), and these pack together as a conventional antiparallel, left-handed coiled-coil. The next level of complexity as we move into the center of the dimer is a left-handed bundle of three helices (orange-red helices in Figure 2A), two of which are parallel and one of which is in an antiparallel configuration. As for the bundle of two helices at the extreme ends of the dimer, this three-helix bundle is formed with residues from the same protomer. Finally, the central segment of the dimer comprises a "six-helix bundle" (blue helices in Figure 2A). Each protomer contributes three helices to the bundle, which associate in an antiparallel fashion and form self-complementary interactions. Knobs-into-holes interactions, such as those found in conventional coiled-coils, occur at each of the helix−helix interfaces.

The same arrangement of helices is shared with the *Drosophila* Amphiphysin and murine Endophilin BAR domains (Figure 2B,C) (*2*, *5*). The helical arrangement of human Arfaptin2 is, however, different from that of the proteins described above (Figure 2D) (*3*). In this case, the central core containing the six-helix bundle structure is much shorter, so that most of the dimer interface of Arfaptin2 corresponds to a region that resembles a "five-helix bundle" (violet in Figure 2D). This results in a slight difference in quaternary structure between Bin1BAR and Arfaptin2, with consequences for their radii of curvature, as discussed below.

The more distantly related IMD domain of IRSp53 has a similar arrangement of helices to the Amphiphysin class, but it contains an extra helix at the C terminus (green in Figure 2E) (*4*) that packs against the 3-helix bundle (orange-red in Figure 2E). Furthermore, the helices leave the central body of the dimer and follow a straight path.

In contrast to the straight helices of IMD, the corresponding helices of Bin1 and endophilin are kinked, and this is most apparent near the structural transition from 6 to 3 helical bundles. For Arfaptin, helix two that is part of each of the 6−5−3−2 helical bundles is smoothly bent without a noticeable kink. Nonetheless, the effect on accumulative curvature of these different proteins is the same for the kinked or smoothly deformed helices.

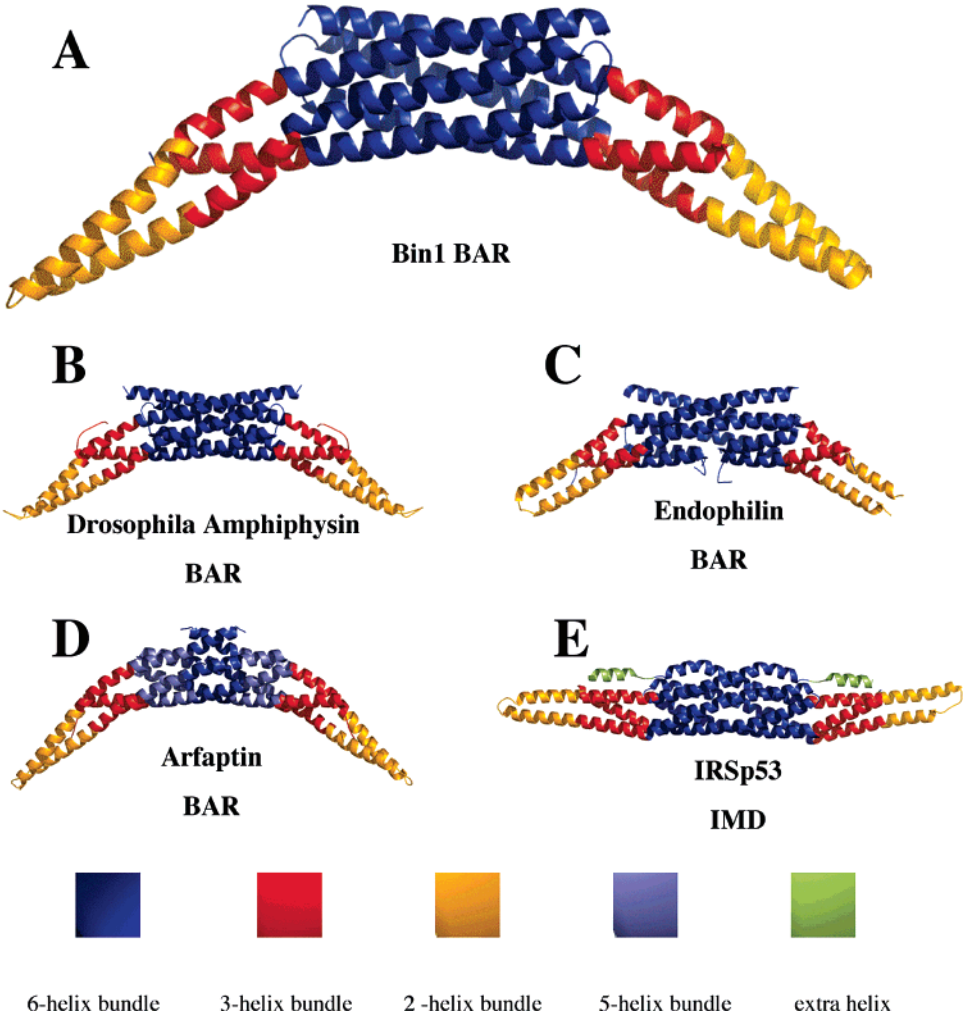

FIGURE 2: Ribbon representation of the different BAR domains of known structure. (A) The helical arrangement in Bin1BAR consists of a central 6-helix bundle (blue), flanked by a 3-helix bundle (orange-red) and, finally, a 2-helix coiled-coil at the periphery (yellow). (B) *Drosophila* Amphiphysin BAR and (C) Endophilin BAR share the same helical arrangement. (D) Arfaptin BAR contains a region that corresponds to a 5-helix bundle (violet). (E) IRSp53 IMD contains an extra helix (green) that associates with the 3-helix bundle (orange-red).

In the *Drosophila* and human Bin1BAR domains, the kink is contributed by a pair of conserved prolines that are conserved among close homologues (corresponding to positions 144 and 207 in the numbering convention for the human BAR; see figure in Supporting Information for a structure-based sequence alignment). A single proline is found on the corresponding helix in endophilin (helix 2), except that it is a helical turn away. This proline occurs at position 142 in endophilin and is strongly conserved among homologues. In the case of Arfaptin, the smooth bending occurs throughout the length of the helix and is more difficult to attribute to a defined sequence pattern.

Analysis of the Curvature and Membrane Binding Potential in BAR Domains. Positively charged amino acids in the second helix and loop regions give the concave face of BAR domain dimers an overall positive electrostatic potential (Figure 3). This face has been proposed to associate with negatively charged phospholipid membranes, and to act as a means of sensing, and in some cases inducing, membrane curvature (*2*).

Positively charged residues in the concave face of Bin1BAR were mutated to negatively charged residues (*2*). These mutations reduced or, when combined, abrogated the tubu-

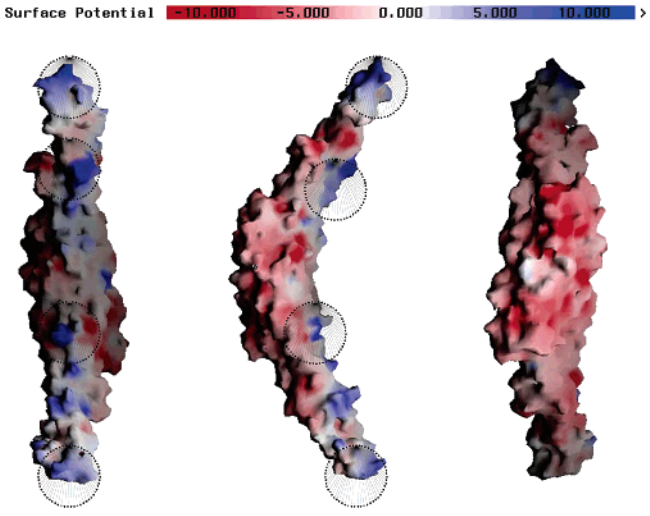

FIGURE 3: Electrostatic potential surface analysis of Bin1BAR using the program GRASP (*32*). Bin1BAR shows the canonical bipartite charge distribution present in other BAR domains: positive charge in the concave face (far left), negative charge in the convex face (far right). The dashed circles indicate the positively charged residues that were mutated in Amphiphysin II and rendered the BAR domain unable to bind to liposomes (*2*).

Table 2: Sequence Identities for Homologues

	Bin1		
	human	Drosophila	Arfaptin
Bin1 *Drosophila*	36.7		
Arfaptin	7.9	8.0	
Endophilin	7.8	7.4	10.0

lation activity and can be mapped to the structure of the Bin1BAR presented here (dashed circles in Figure 3). As predicted, they lie on the face speculated to engage with membranes, supporting the proposed mode of membrane binding and bending for BAR domains.

In contrast to the concave face, the convex face displays a negatively charged surface (Figure 3). This bipartite polarity could aid in the alignment of BAR domains on membranes and perhaps favor the packing of neighboring domains to form the smooth, cylindrical tubule-like structures observed *in vivo* and *in vitro* without any "dimple" distortion of the engaged surface. It is interesting to note that all BAR domains seem to display this charge distribution pattern, including those for which membrane association is not a demonstrated aspect of their function, such as the IMD domain of IRSp53 (*2*−*5*).

The Bin1BAR dimer would fit a sphere of 220 Å diameter, with its molecular 2-fold axis normal to the spherical surface. The curvature of the dimer results from the way that the monomers intersect and also from the kinks in helices 2 and 3 caused by two prolines (residues 144 and 207). The same radius of curvature is observed in *Drosophila* Amphiphysin and Endophilin BAR domain structures (without taking into consideration the insertion in the concave face that occurs in endophilin BAR domain, which has been suggested to match a membrane of 300 Å diameter) (*2*, *5*). The larger radius of curvature for endophilin is extrapolated from the predicted location of the highly mobile insertion; however, this portion may not affect the surface curvature from the typical value of 220 Å if it is inserted into the membrane or distributed over the surface (see Note Added in Proof). This is shown in a superposition of Bin1BAR with the two other structures (Figure 4A,B). Just as described for the Bin1BAR domain, the curvature in these proteins is caused both by the way the protomers intersect and by the kinks in the helices as the domains make the transition between helical bundles. Thus, the BAR domains from the three Bin1, *Drosophila* Amphiphysin, and Endophilin proteins have similar surface curvature, with similar electrostatic distributions, and may all recognize a complementary target surface in similar ways.

However, not all BAR domain structures share the same curvature. The curvature of the Arfaptin2 BAR domain differs markedly from that of the Amphiphysin type described above (*3*). This is shown in a structural overlay where one protomer from each dimer (Bin1BAR and Arfaptin) has been used as the common reference frame (Figure 4C i−iii). In comparison to the Amphiphysin class of BAR domain, which would fit a circle of diameter 220 Å, the Arfaptin2 BAR domain structure would fit a tighter circle of only 150 Å in diameter. Since the Bin1BAR and Arfaptin2 protomers are structurally similar (Figure 4C iv), the difference in radius of curvature between the dimers arises from the relative orientation of the interacting protomers. If we imagine the dimer to be like a pair of scissors, then the Bin1BAR domain might be described as more "open" than Arfaptin2 BAR. This arises from the slightly different orientation of the helices in the five-helix bundle of Arfaptin *versus* the comparatively straighter six-helix bundle of Bin1 (Figure 2).

In contrast to Arfaptin2, the IMD domain of IRSp53 is more open than Bin1BAR (*4*) and appears completely straight. When the two proteins are superimposed using the dimer interface as the reference frame, the two central regions match remarkably well (Figure 4D i−iii). However, when the single protomers are superimposed, the extreme ends of the monomers bend in opposite directions, due to kinks caused by proline residues at different positions (Figure 4D iv). Moreover in IRSp53 this different structure appears to be stabilized by the binding of a small C-terminal helix. Therefore, when comparing IRSp53 and Bin1BAR structures, it is the curvature of the protomers themselves, rather than the way in which they intersect, that is different.

Potential for Protein−*Protein Interactions.* The structure of the BAR domain of Arfaptin in complex with the small G-protein Rac reveals that the interaction occludes the concave surface of Arfaptin BAR (*3*). A functional relationship between Amphiphysins and the signaling pathways mediated by the small G-protein Rab5 has been suggested (*15*, *41*), and a link between other BAR proteins and small G-proteins has also been proposed (*20*). This prompted us to investigate whether Bin1BAR may bind Rab5 in a manner analogous to the Arfaptin2−Rac interaction, using a computational approach.

The surfaces of Bin1BAR and ArfaptinBAR were analyzed with an algorithm that evaluates propensity for protein−protein interactions based on the desolvation energy, known as the optimal docking area (ODA) (*29*). The method calculates the effective desolvation energy of burying a surface patch from the solvent, based on atomic solvation parameters (ASPs) optimized for protein−protein docking (*42*). As a test of the method, the first set of calculations were undertaken with the isolated Bin1BAR protomers, and they successfully predicted the observed dimerization interfaces (Figure 5A). When calculations were undertaken for the Arfaptin2 BAR dimer, the binding interface for Rac was also predicted accurately (Figure 5C). Significantly, the corresponding region is not predicted to be a protein−protein interaction site in the Bin1BAR dimer (Figure 5B). This analysis suggests that Bin1BAR lacks the capacity to bind small G-proteins in the same way as seen in the Arfaptin−Rac interaction. In addition, *in vitro* binding studies performed between human Bin1BAR and several human small Rab proteins also failed to detect an interaction at micromolar concentrations (details in Experimental Procedures).

Two regions with weak potential for protein−protein interaction were nevertheless detected in Bin1BAR (arrows in Figure 6A). These regions occur on the convex face of the domain, at the point where the structural transition occurs from the six-helix to the three-helix bundle; there are two such sites that are related by molecular symmetry. The same ODA calculations were performed on *Drosophila* Amphiphysin, Endophilin A1, and Arfaptin2, and analogous regions with propensity for protein−protein interactions were detected (Figure 6B−D, regions marked with arrows). Even though the propensity is weak for the Bin1BAR and *Drosophila* Amphiphysin domains, the fact that the sites are

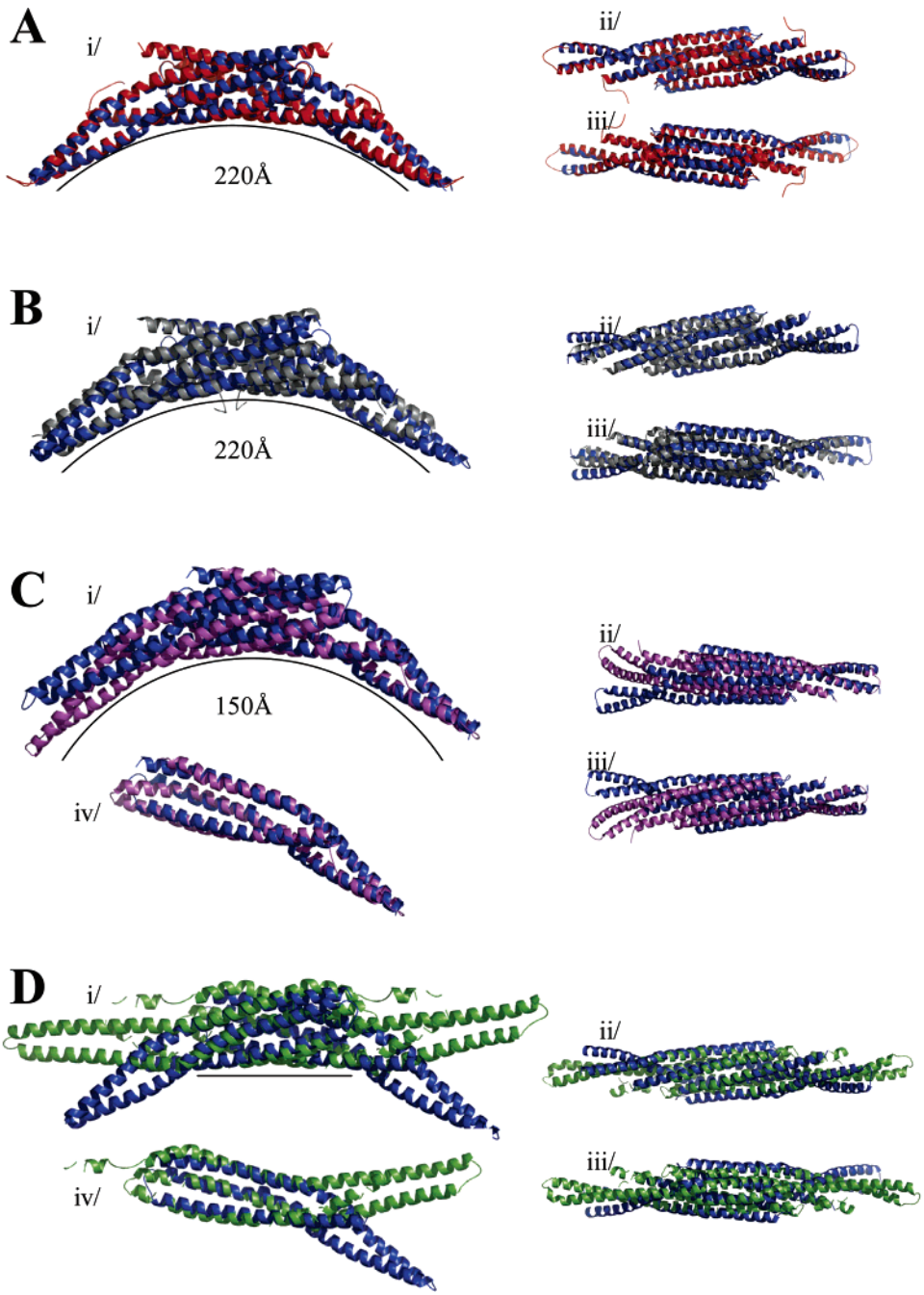

FIGURE 4: Comparison of the curvature of Bin1BAR with other BAR domains of known structure. Curvatures were compared by superposing the structure of Bin1BAR (navy blue) with all the other structures. The numbers i, ii, and iii correspond to the side, concave, and convex views of the dimer, respectively. Number iv corresponds to the superpositions of the protomers alone, where appropriate. (A) Bin1BAR dimer (blue) superposed with *Drosophila* Amphiphysin BAR (red). (B) Bin1BAR dimer (blue) superposed with Endophilin BAR (gray). (C) Bin1BAR dimer (blue) superposed with Arfaptin 2 BAR (pink). (D) Bin1BAR (blue) superposed with the IMD domain of IRSp53 (green).

conserved suggests that they might be a general feature of the family. It is not likely that the residues lacking from the N-terminus are affecting the ODA results, because the residues with lowest ODA values are not close to the N-terminus. We propose that these sites are interaction or regulatory sites in a subset of BAR domain proteins. This surface could form interdomain interactions in the full-length proteins, given its proximity to the terminus of the BAR domain structure. Since these sites are located at the convex face of the dimer, they would not interfere with membrane binding that is suggested to be the central function of Bin1, Endophilin, and Amphiphysin. Corresponding interaction sites are not present in the more distantly related IMD of IRSp53, but there is an extra C-terminal extension that masks the putative binding site (Figure 6E). Interestingly, in the IMD of IRSp53, a site analogous to the Rac-binding site of Arfaptin2 is predicted (Figure 6E). IRSp53 has been shown to interact with the small G-protein Rac and the Rac regulatory protein Wave, even though the specific sites of the interaction have not been mapped (*22*). We speculate that the IMD domain of IRSp53 interacts with G-proteins in the same way as in the Arfaptin−Rac complex.

Other Bin1/Amphiphysin II Isoforms. Although there are differences in the structure and function of the central nervous

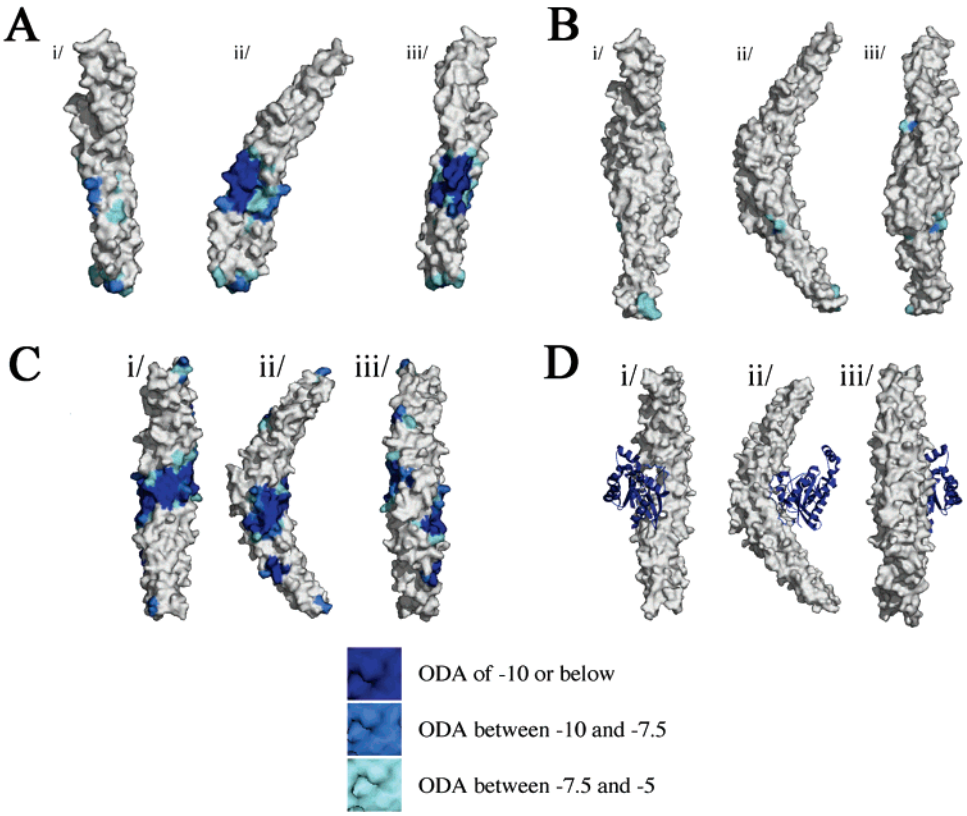

FIGURE 5: Optimal docking area (ODA) analysis of Bin1BAR and Arfaptin2 BAR. The difference between the proteins indicates that Bin1BAR is unlikely to engage in interactions with G-proteins. The numbers i, ii, and iii correspond to the concave, side, and convex views of the dimer, respectively. (A) ODA analysis for a Bin1BAR protomer. As can be seen from the dark blue patches, the dimerization interface in the protomer is clearly predicted with this analysis. (B) ODA analysis for the Bin1BAR dimer. The concave face of the Bin1BAR dimer has no predicted propensity for protein interaction. (C) ODA analysis for the Arfaptin2 BAR dimer. (D) Structure of Arfaptin2 BAR (white) in complex with Rac (blue). A comparison of panels C and D clearly indicates that the binding site for Rac in Arfaptin is correctly predicted by the ODA calculations.

system isoforms (termed Amphiphysin II isoforms) and the ubiquitous isoforms and muscle isoforms (termed Bin1 isoforms), all the Bin1/Amphiphysin II isoforms share the same domain organization at the extreme ends of the protein, i.e., the N-terminal BAR domain and the C-terminal SH3 domain. In some Amphiphysin II isoforms found in the brain and central nervous system, the BAR domain includes an insertion of 31 residues at amino acid position 173, resulting from alternate splicing (between helices 2 and 3). This insertion distinguishes Amphiphysin II splice variants from the human Amphiphysin I and *Drosophila* Amphiphysin. However, we expect that the insertion will not affect curvatures and archectures, although it may affect function. Endophilin B1 is expected to have an insertion similar to that found in Amphiphysin II, judging from a reported structure-based sequence alignment (*5*).

Secondary structure predictions (*43*) indicate that this region forms a helix. Based on the sequence alone, we have prepared a model with a helical insertion (Figure 7A). Electrostatic analysis of the model suggests that isoforms carrying this insertion have a markedly more electropositive concave face, and the insertion may thus strengthen the interaction of the domain with membranes (Figure 7B). All the isoforms that carry this insertion are likely to be expressed in the central nervous system and to function in endocytosis or vesicle trafficking. In addition, ODA analysis predicts that this region contains a strong potential for mediating protein−protein interactions (Figure 7C). However, whether this insertion is used for specialized interactions with membranes or components of the endocytic or vesicle trafficking machinery is at this point unknown. As noted above, the protein encoded by the single Amphiphysin gene in the *Drosophila* genome (*44*) is believed to be more similar to the ubiquitous human Bin1 isoforms that lack this insertion than to mammalian Amphiphysin I or Amphiphysin II isoforms expressed in the central nervous system. *Drosophila* Amphiphysin therefore also lacks the 31 amino acid insertion in the BAR domain, and is dispensable for endocytosis and expressed predominantly in muscle, consistent with the notion that its function resembles one of the ubiquitous Bin1 isoforms (*16*−*18*).

DISCUSSION

BAR and IMD domains constitute a family of elongated coiled-coiled dimers with varying degrees of curvature. Members of this family all share a bipartite distribution of electrostatic surface potential that would support a membrane binding role. However, it is also very likely that certain subclasses of BAR domains may not have a membrane-binding function, but instead play other roles involving protein−protein interactions. Here, we have solved and examined the crystal structure of the BAR domain of human Bin1, and compared it to other reported BAR-domain structures. Based on our analysis of the curvature, and potential for protein−protein interactions, we propose a structural classification of the BAR-domain family.

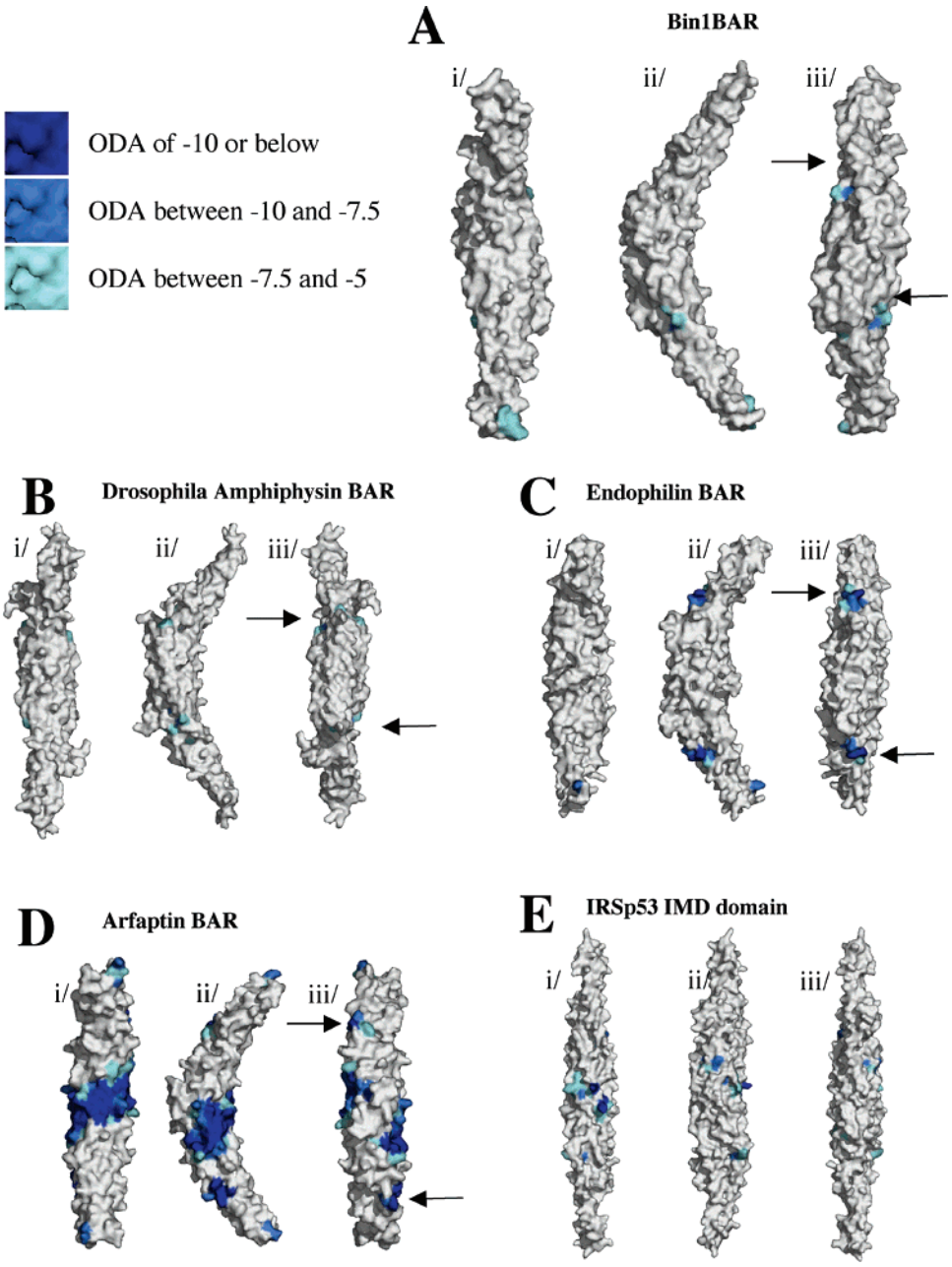

FIGURE 6: Optimal docking area (ODA) analysis of BAR domain structures and of the IMD domain structure of IRSp53. The numbers i, ii, and iii correspond to the concave, side, and convex views of the dimer, respectively. (A) Bin1BAR, (B) *Drosophila* Amphiphysin BAR, (C) Endophilin BAR, (D) Arfaptin BAR, and (E) IMD domain of IRSp53. BAR domains from panels A to D possess a predicted site with potential for protein−protein interactions on the convex face of the dimer (shown as arrows in iii). For some BAR domains, this potential is strong, such as in endophilin BAR and Arfaptin BAR (C and D) while in the amphiphysins (A and B) it is only weak. This site does not seem to be present in the IMD domain of IRSp53 (E). However, a site analogous to Arfaptin's Rac interaction site in the concave face is predicted.

From our observations, the BAR/IMD family can be divided into at least three architectural classes on the basis of their structures and curvatures; these will have implications for their distinctive biological roles and potential for protein−protein interactions:

1. The Amphiphysin-Type Class of BAR Domains, Encompassing Bin1BAR, Drosophila Amphiphysin, and Endophilin. The main features of the class include the ability to tubulate membranes, the ability to match a circle of ~220 Å diameter, and two potential protein interaction sites on the convex face of the dimer. A kink that contributes to the curvature is correlated with a pair of conserved prolines corresponding to positions 144 and 207 in the numbering convention for the human BAR. A single proline is found at position 142 on the corresponding helix in endophilin (helix 2) and is strongly conserved among homologues. We note that, because of its mobile protusions, the Endophilin A1 BAR would be expected to be distinct within this group in regard to function. (See Note Added in Proof.)

2. The Arfaptin Class. So far, this is based on the Arfaptin protein alone. The protein is characterized by a smaller radius of curvature that would fit a circle ~150 Å in diameter, and its direct association with membranes is yet to be established. However, it contains a protein interaction site in the center of the concave face of the dimer, and two possible symmetrical interaction sites on the convex face analogous to

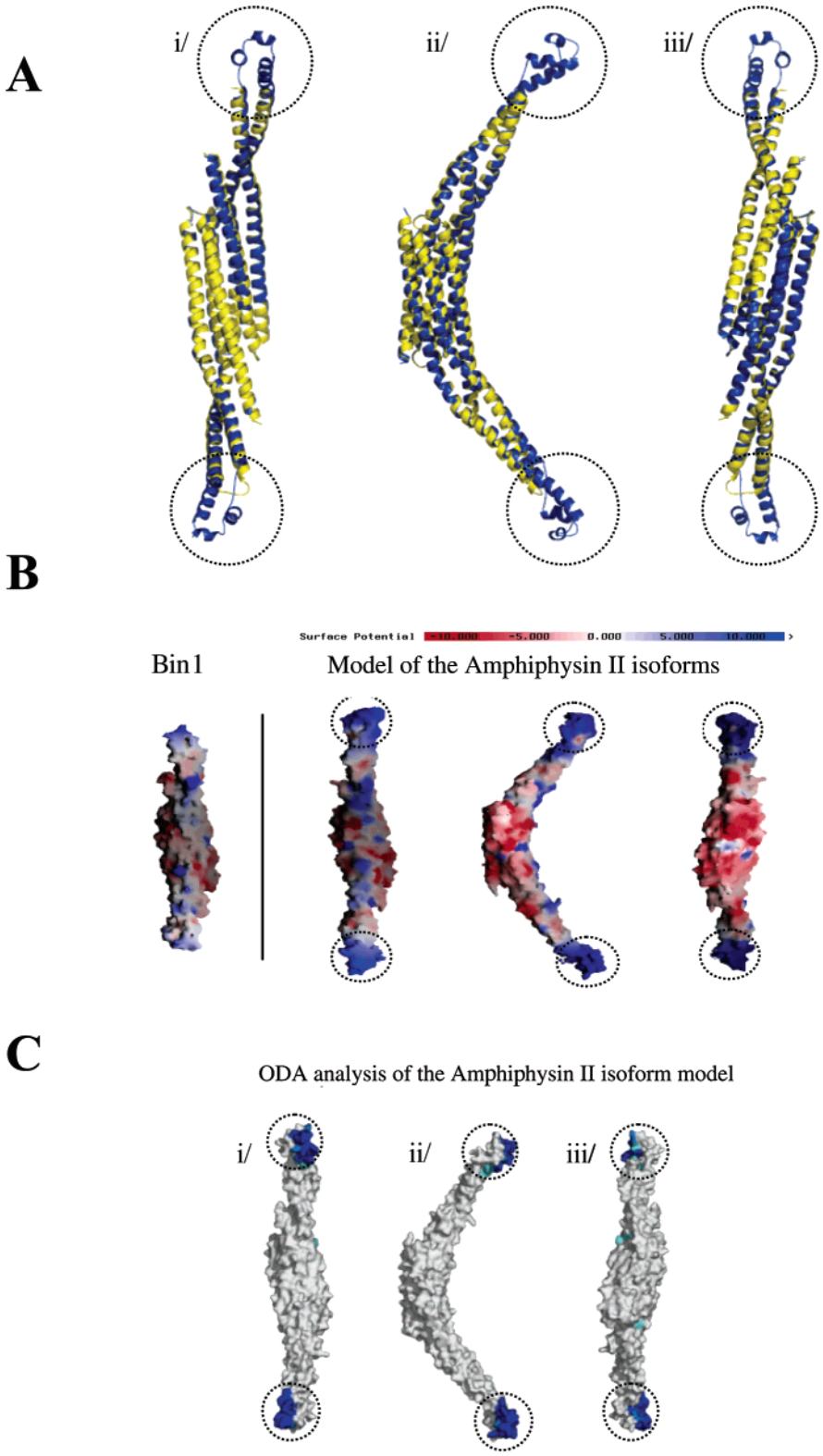

FIGURE 7: (A) The structure of the mammalian Amphiphysin II model (dark blue) superimposed to the Bin1 isoform structure (Bin1BAR) (yellow). The modeled insertion region is highlighted with a dashed circle. The numbers i, ii, and iii correspond to the concave, side, and convex views of the dimer, respectively. (B) Electrostatic analysis of the model. (C) ODA analysis of the model.

that found in the Amphiphysin class. Unlike the Amphiphysin-like class mentioned above, there are no apparent kinks in the helices that contribute to the curvature; instead, a long central helix that is smoothly bent occurs throughout its length, and this is likely caused by a distributed sequence effect in contrast to a more defined sequence pattern.

3. The IMD Domain Class. As with the Arfaptin class, the direct association of this domain with membranes is yet to be established, although the protein is clearly involved in membrane remodeling events. It is characterized by a straight shape with no curvature, and a potential for protein interactions on the concave face of the dimer equivalent to

Arfaptin2. The convex face of the dimer does not seem to have any interaction site analogous to those in the Amphiphysin and Arfaptin classes, although these sites could be potentially masked by the additional C-terminal helix.

We have described here how different BAR domain classes have different curvatures, and how this originates from knobs-into-holes interactions that influence both quaternary and tertiary organization. Many BAR domain containing proteins induce tubulation of liposomes *in vitro*, but these tubules can vary in radii from 200 to 1000 Å, even for the same protein. One puzzle is how the varying radii might arise if the curvature of the BAR domain determines the induced membrane curvature. We note that a macromolecular assemblage as extensive as a tubule is likely to be formed by great numbers of BAR proteins, which could for instance make protein−protein interactions to generate parallel, coaxial filaments on the surface of the tubule and cause its radius to expand. Another possibility is that other regions of BAR proteins may also interact with membranes and so effect the macroscopic curvature.

Functional diversity of BAR domains can be generated through inserted regions. For example, Endophilin contains an insertion on the concave face (*5*), while certain Amphiphysin II isoforms have insertions at the extreme ends of the dimer that are expected to change the properties of the dimer, as indicated in the model presented here. Many BAR domains contain an additional N-terminal helix that enhances the membrane binding ability of the BAR domain (*2*). All the differences will clearly have a major impact on the properties of the proteins, and in many cases, a combination of characteristics may be used to tailor the protein for a particular cellular function.

Note Added in Proof. The crystal structure of human endophilin BAR domain has been reported and reveals a pair of helices inserted on the center of the concave face of the dimer (*45*). The authors present functional data that show that these helices become inserted into the membrane to facilitate membrane curvature, and they also provide evidence that rigidity of the crescent shape is required for causing tubulation, but not vesicle formation.

ACKNOWLEDGMENT

We thank the staff of the ESRF and Daresbury SRS Laboratory for use of synchrotron facilities. We are grateful to Venkatesh Pratap and Kenji Mizuguchi for helpful discussions.

SUPPORTING INFORMATION AVAILABLE

Figure for structure based sequence alignment. This material is available free of charge via the Internet at http://pubs.acs.org.

REFERENCES

1. Sakamuro, D., Elliott, K. J., Wechsler-Reya, R., and Prendergast, G. C. (1996) BIN1 is a novel MYC-interacting protein with features of a tumour suppressor, *Nat. Genet. 14*, 69−77.
2. Peter, B. J., Kent, H. M., Mills, I. G., Vallis, Y., Butler, P. J., Evans, P. R., and McMahon, H. T. (2004) BAR domains as sensors of membrane curvature: the amphiphysin BAR structure, *Science 303*, 495−9.
3. Tarricone, C., Xiao, B., Justin, N., Walker, P. A., Rittinger, K., Gamblin, S. J., and Smerdon, S. J. (2001) The structural basis of Arfaptin-mediated cross-talk between Rac and Arf signalling pathways, *Nature 411*, 215−9.
4. Millard, T. H., Bompard, G., Heung, M. Y., Dafforn, T. R., Scott, D. J., Machesky, L. M., and Futterer, K. (2005) Structural basis of filopodia formation induced by the IRSp53/MIM homology domain of human IRSp53, *EMBO J. 24*, 240−50.
5. Weissenhorn, W. (2005) Crystal structure of the endophilin-A1 BAR domain, *J. Mol. Biol. 351*, 653−61.
6. Lee, E., Marcucci, M., Daniell, L., Pypaert, M., Weisz, O. A., Ochoa, G. C., Farsad, K., Wenk, M. R., and De Camilli, P. (2002) Amphiphysin 2 (Bin1) and T-tubule biogenesis in muscle, *Science 297*, 1193−6.
7. Farsad, K., Ringstad, N., Takei, K., Floyd, S. R., Rose, K., De Camilli, P. (2001) Generation of high curvature membranes mediated by direct endophilin bilayer interactions, *Cell Biol. 155*, 193−200.
8. Zhang, B., and Zelhof, A. C. (2002) Amphiphysins: raising the BAR for synaptic vesicle recycling and membrane dynamics. Bin-Amphiphysin-Rvsp, *Traffic 3*, 452−60.
9. Yamamoto, R., Li, X., Winter, S., Francke, U., Kilimann, M. W. (1995) Primary structure of human amphiphysin, the dominant autoantigen of paraneoplastic stiff-man syndrome, and mapping of its gene (AMPH) to chromosome 7p13-p14, *Hum. Mol. Genet. 4*, 265−8.
10. Leprince, C., Le Scolan, E., Meunier, B., Fraisier, V., Brandon, N., De Gunzburg, J., and Camonis, J. (2003) Sorting nexin 4 and amphiphysin 2, a new partnership between endocytosis and intracellular trafficking, *J. Cell Sci. 116*, 1937−48.
11. Butler, M. H., David, C., Ochoa, G. C., Freyberg, Z., Daniell, L., Grabs, D., Cremona, O., and De Camilli, P. (1997) Amphiphysin II (SH3P9; BIN1), a member of the amphiphysin/Rvs family, is concentrated in the cortical cytomatrix of axon initial segments and nodes of ranvier in brain and around T tubules in skeletal muscle, *J. Cell Biol. 137*, 1355−67.
12. Tsutsui, K., Maeda, Y., Tsutsui, K., Seki, S., and Tokunaga, A. (1997) cDNA cloning of a novel amphiphysin isoform and tissue-specific expression of its multiple splice variants, *Biochem. Biophys. Res. Commun. 236*, 178−83.
13. Wechsler-Reya, R., Sakamuro, D., Zhang, J., Duhadaway, J., and Prendergast, G. C. (1997) Structural analysis of the human BIN1 gene. Evidence for tissue-specific transcriptional regulation and alternate RNA splicing, *J. Biol. Chem. 272*, 31453−8.
14. Wechsler-Reya, R. J., Elliott, K. J., and Prendergast, G. C. (1998) A role for the putative tumor suppressor Bin1 in muscle cell differentiation, *Mol. Cell. Biol. 18*, 566−75.
15. Kajiho, H., Saito, K., Tsujita, K., Kontani, K., Araki, Y., Kurosu, H., and Katada, T. (2003) RIN3: a novel Rab5 GEF interacting with amphiphysin II involved in the early endocytic pathway, *J. Cell Sci. 116*, 4159−68.
16. Razzaq, A., Robinson, I. M., McMahon, H. T., Skepper, J. N., Su, Y., Zelhof, A. C., Jackson, A. P., Gay, N. J., and O'Kane, C. J. (2001) Amphiphysin is necessary for organization of the excitation-contraction coupling machinery of muscles, but not for synaptic vesicle endocytosis in Drosophila, *Genes Dev. 15*, 2967−79.
17. Leventis, P. A., Chow, B. M., Stewart, B. A., Iyengar, B., Campos, A. R., and Boulianne, G. L. (2001) Drosophila Amphiphysin is a post-synaptic protein required for normal locomotion but not endocytosis, *Traffic 2*, 839−50.
18. Zelhof, A. C., Bao, H., Hardy, R. W., Razzaq, A., Zhang, B., and Doe, C. (2001) Drosophila Amphiphysin is implicated in protein localization and membrane morphogenesis but not in synaptic vesicle endocytosis, *Development 128*, 5005−15.
19. Muller, A. J., Baker, J. F., DuHadaway, J. B., Ge, K., Farmer, G., Donover, P. S., Meade, R., Reid, C., Grzanna, R., Roach, A. H., Shah, N., Soler, A. P., and Prendergast, G. C. (2003) Disruption of the murine Bin1/Amphiphysin II gene does not disable endocytosis but results in embryonic cardiomyopathy with aberrant myofibril formation, *Mol. Cell. Biol. 23*, 4295−306.
20. Habermann, B. (2004) The BAR-domain family of proteins: a case of bending and binding?, *EMBO Rep. 5*, 250−5.
21. Miaczynska, M., Christoforidis, S., Giner, A., Shevchenko, A., Uttenweiler-Joseph, S., Habermann, B., Wilm, M., Parton, R. G., and Zerial, M. (2004) APPL proteins link Rab5 to nuclear signal transduction via an endosomal compartment, *Cell 116*, 445−56.
22. Miki, H., Yamaguchi, H., Suetsugu, S., and Takenawa, T. (2000) IRSp53 is an essential intermediate between Rac and WAVE in the regulation of membrane ruffling, *Nature 408*, 732−5.

23. Owen, D., Lowe, P. N., Nietlispach, D., Brosnan, C. E., Chirgadze, D. Y., Parker, P. J., Blundell, T. L., and Mott, H. R. (2003). Molecular dissection of the interaction between the small G proteins Rac1 and RhoA and protein kinase C-related kinase 1 (PAK1), *J. Biol. Chem. 278*, 50578−87.
24. Otwinowski, Z., and Minor, W. (1997) *Methods Enzymol. 276*, 307−26.
25. Vagin, A., and Teplyakov, A. (2000) An approach to multi-copy search in molecular replacement, *Acta Crystallogr., D: Biol. Crystallogr. 56*, 1622−4.
26. Brunger, A. T., Adams, P. D., Clore, G. M., DeLano, W. L., Gros, P., Grosse-Kunstleve, R. W., Jiang, J. S., Kuszewski, J., Nilges, M., Pannu, N. S., Read, R. J., Rice, L. M., Simonson, T., and Warren, G. L. (1998) Crystallography & NMR system: A new software suite for macromolecular structure determination, *Acta Crystallogr., D: Biol. Crystallogr. 54*, 905−21.
27. Murshudov, G. N., Vagin, A. A., Lebedev, A., Wilson, K. S., and Dodson, E. J. (1999) Efficient anisotropic refinement of macromolecular structures using FFT, *Acta Crystallogr., D: Biol. Crystallogr. 55*, 247−55.
28. Emsley, P., and Cowtan, K. (2004) Coot: model-building tools for molecular graphics, *Acta Crystallogr., D: Biol. Crystallogr. 60*, 2126−32.
29. Fernandez-Recio, J., Totrov, M., Skorodumov, C., and Abagyan, R. (2005) Optimal docking area: a new method for predicting protein-protein interaction sites, *Proteins 58*, 134−43.
30. Walshaw, J., and Woolfson, D. N. (2001) SOCKET: A Program for Identifying and Analysing Coiled-coil Motifs Within Protein Structures, *J. Mol. Biol. 307*, 1427−50.
31. Cohen, G. H. (1997) ALIGN: a program to superimpose protein coordinates, accounting for insertions and deletions, *J. Appl. Crystallogr. 30*, 1160−1.
32. Nicholls, A., Sharp, K., and Honig, B. (1991) Protein folding and association: insights from the interfacial and thermodynamic properties of hydrocarbons, *Proteins 11*, 281−96.
33. DeLano, W. L. (2002) The PyMOL molecular graphics system. http://www.pymol.org.
34. Shi, J., Blundell, T. L., and Mizuguchi, K. (2001) FUGUE: sequence-structure homology recognition using environment-specific substitution tables and structure-dependent gap penalties, *J. Mol. Biol. 310*, 243−57.
35. Pandit, J., Danley, D. E., Schulte, G. K., Mazzalupo, S. M., Pauly, T. A., Hayward, C. M., Hamanaka, E. S., Thompson, J. F., and Harwood, H. J. (2000) Crystal structure of human squalene synthase. A key enzyme in cholesterol biosynthesis, *J. Biol. Chem. 275*, 30610−7.
36. Fiser, A., and Sali, A. (2003) Modeller: generation and refinement of homology-based protein structure models, *Methods Enzymol. 374*, 461−91.
37. Canutescu, A. A., Shelenkov, A. A., and Dunbrack, R. L., Jr. (2003) A graph theory algorithm for protein side-chain prediction, *Protein Sci. 12*, 2001−14.
38. Laskowsky, R. A., MacArthur, M. W., Moss, D. S., and Thornton, J. R. (1993) PROCHECK−A program to check the stereochemical quality of protein structures, *J. Appl. Crystallogr. 26*, 283−91.
39. Luthy, R., Bowie, J. U., and Eisenberg, D. (1992) Assessment of protein models with three-dimensional profiles, *Nature 356*, 83−5.
40. Davis, I. W., Murray, L. W., Richardson, J. S., and Richardson, D. C. (2004) MOLPROBITY: structure validation and all-atom contact analysis for nucleic acids and their complexes, *Nucleic Acids Res. 32* (Web Server issue), W615−9.
41. Talarek, N., Balguerie, A., Aigle, M., and Durrens, P. (2005) A novel link between a Rab GTPase and Rvs proteins: the yeast amphiphysin homologues, *Cell Biochem. Funct. 23*, 253−66.
42. Fernandez-Recio, J., Totrov, M., and Abagyan, R. (2004) Identification of protein-protein interaction sites from docking energy landscapes, *J. Mol. Biol. 335*, 843−65.
43. Cuff, J. A., Clamp, M. E., Siddiqui, A. S., Finlay, M., and Barton, G. J. (1998) Jpred: A Consensus Secondary Structure Prediction Server, *Bioinformatics 14*, 892−3.
44. Razzaq, A., Su, Y., Mehren, J. E., Mizuguchi, K., Jackson, A. P., Gay, N. J., and O'Kane, C. J. (2000) Characterisation of the gene for Drosophila amphiphysin, *Gene 24*, 167−74.
45. Masuda, M., Takeda, S., Sone, M., Ohki, T., Mori, H., Kamioka, Y., and Mochizuki, N. (2006) Endophilin Bar domain drives membrane curvature by two newly identified structure-based mechanisms, *EMBO J. 25*, 2889−97.

BI060717K